EUROPEAN ORGANIZATION FOR NUCLEAR RESEARCH

Proposal to the ISOLDE and Neutron Time-of-Flight Committee

Emission channeling with short-lived isotopes (EC-SLI) of acceptor dopants in nitride semiconductors

10.1.2017

U. Wahl[1], V. Augustyns[2], J.G. Correia[1], A. Costa[1], E. David Bosne[1], T.A.L. Lima[2], G. Lippertz[2], L.M.C. Pereira[2], M.R. da Silva[3], K. Temst[2], and A. Vantomme[2]
(The EC-SLI collaboration)

1 Centro de Ciências e Tecnologias Nucleares (C2TN), Instituto Superior Técnico, Universidade de Lisboa, 2695-066 Bobadela, Portugal
2 KU Leuven, Instituut voor Kern- en Stralingsfysica (IKS), 3001 Leuven, Belgium
3 Centro de Física Nuclear da Universidade de Lisboa (CFNUL), 1649-003 Lisboa, Portugal

Spokesperson: U. Wahl (Ulrich.Wahl@cern.ch)
Local contact: J.G. Correia (Guilherme.Correia@cern.ch)

CERN-INTC-2017-003 / INTC-P-489
10/01/2017

Abstract

Despite the overwhelming technological success of GaN-related devices in optoelectronics, the detailed structure of possible acceptor impurities in nitride semiconductors has been heavily debated ever since the realization of *p*-type GaN through Mg doping by Akasaki, Amano, and Nakamura in 1989-1992.

The implementation of the Emission Channeling with Short-Lived Isotopes (EC-SLI) lattice location method with ^{27}Mg($t_{1/2}$=9.45 min) and ^{11}Be ($t_{1/2}$=13.8 s) at ISOLDE has now for the first time provided an experimental technique for direct study of the structural properties of Mg and Be in nitrides. While this has already lead to valuable results, including direct evidence for the existence of interstitial Mg and Be, the fact that interstitial and substitutional fractions of these implanted probes can now be detected with the precision of a few %, opens further possibilities of investigating how electrical activation processes and radiation damage influence these quantities in differently doped GaN samples.

As further studies using ^{27}Mg we propose to concentrate on detailed mapping of the site change from interstitial to substitutional Ga sites in different doping types of GaN (nid-GaN, GaN:Mg, *p*-GaN:Mg, *n*-GaN:Si,) as a function of implantation temperature and fluence.

In the case of ^{11}Be, where so far we could only achieve room temperature results in GaN, we aim at establishing the temperatures where the site changes from interstitial to substitutional positions occur in nid-GaN, *p*-GaN:Mg and AlN.

Requested shifts: **24 (split into 3 runs over 2 years)**

Motivation

Mg-doped *p*-type GaN is nowadays a core component of many optoelectronic devices which we find in our homes, e.g. light emitting diodes (LEDs) for solid state white lighting or blue lasers [1-3]. Applications of GaN for power electronics, e.g. as high voltage transistors or power converters, also exist already but are less widespread; others, as in photovoltaics may still emerge. Despite the technological maturity of GaN, there are some basic properties related to its *p*-type doping that are still poorly understood and also limit the performance of devices. One such major problem is an inherent doping limit: once the Mg concentration in GaN surpasses ~10^{19}–10^{20} cm^{-3}, further introduction of Mg does not lead to an increase in the hole concentration, see e.g. Ref. [4] and Refs. therein. The electrical activation of Mg as a *p*-type dopant requires its incorporation on the substitutional Ga site S_{Ga} (Mg_{Ga}) while Mg on other sites, e.g. interstitial Mg (Mg_i), or Mg replacing N (Mg_N), should be electrically inactive or even exhibit donor character. In the earlier stages of GaN research it was suggested from ab initio density functional theory calculations by Neugebauer and Van de Walle [5-6] that "incorporation of the Mg atoms on the N site or in an interstitial configuration were found to be negligible." This view, however, was not shared by all theorists, e.g. Reboredo and Pantelides stated that "interstitial Mg plays a major role in limiting *p*-type doping" [7]. The failure of experimental methods in establishing the existence of interstitial Mg and investigating its properties probably contributed to the fact that in the following years many researchers adopted the opinion that the doping limitations at high Mg concentrations are, in addition to passivation by H [1-3,6,8], mostly a consequence of native defects with donor character, in particular N vacancies V_N, either in their isolated form [9-10] or in Mg_{Ga}-V_N complexes with Mg [11-12].

Recently this controversial discussion was revived by the results of hybrid density functional calculations of Miceli and Pasquarello [13] who concluded that "…the amphoteric nature of the Mg impurity is critical to explain the dropoff in the hole density observed experimentally": once the doping limit has been reached, additional Mg atoms are not incorporated on substitutional Ga sites any more but on interstitial sites where they form compensating double donors, thus pinning the Fermi level, cf Ref. [13] for a more detailed discussion of several arguments that support this theory from the viewpoint of electrical and optical characterization methods. Low formation energies for interstitial Mg_i if the Fermi level is located below mid gap were also theoretically predicted by Reshchikov *et al.* [14].

For the lighter alkaline earth metal Be, theory has not reached a consensus whether in GaN its acceptor energy is similar to Mg [6,10,15-16] or much higher [17-18]. It has also been suggested that Be suffers to larger extent than Mg from self-compensation in the form of Be_i interstitials [6,15-16]. In the case of the extremely wide band gap material AlN, the quest for *p*-type AlN has not been successful and besides a deep nature of Mg and Be acceptors [18] compensation by interstitials may also play a leading role.

In contrast to the various refined but often contradictory theoretical models on the structural properties of Mg- and Be-related defects in GaN, no experimental data on the Mg and Be lattice sites existed so far. The often used ion beam lattice location technique of Rutherford backscattering spectrometry/channeling (RBS/C) is not applicable in this case since Mg and Be are much lighter than the Ga host atoms. Alternative ion beam detection methods such as particle-induced X-ray emission (PIXE) or nuclear reaction analysis fail at the low concentrations of dopants. Attempts to use extended X-ray absorption fine structure (EXAFS) for characterizing the distances from Mg atoms to their nearest neighbors were not successful since the Mg K X-ray absorption edge overlaps with the Ga L-edge [19].

Summary of previous results

Within our previous experiment IS453 we have recently provided first direct lattice location measurements for ^{27}Mg ($t_{1/2}$=9.5 min) in AlN [20-21] and GaN [20,22] using the β^- emission

channeling technique with short-lived isotopes (EC-SLI). We found that the majority of ion-implanted Mg occupies substitutional Ga or Al sites. However, we presented also direct experimental proof for the existence of interstitial Mg_i on positions near the so-called octahedral sites. In the case of GaN we could show that the interstitial Mg fraction depends on the GaN doping character, being enhanced in samples that were pre-doped *p*-type with stable Mg during growth, and suppressed in Si-doped *n*-GaN, which was recently accepted in Phys. Rev. Lett. [22]

The EC-SLI method allows probing the sites of radioactive isotopes in single-crystalline samples [23-25]. The radioactive probe atoms are implanted at low fluence and the emitted β^- particles are guided by the crystal potential. Within our on-line setup [26] at the GHM beam line, a two-dimensional position-sensitive detector (PSD) [24-25] is used to measure the angle-dependent emission yield of electrons in the vicinity of major crystallographic directions, providing patterns which are characteristic for the probe atom sites in the sample. In order to derive the fractions of probe atoms on different lattice sites, the experimental β^- emission yields are fitted by a linear combination of theoretical patterns corresponding to emitter atoms residing on different lattice sites. The theoretical β^- patterns are calculated using the so-called "manybeam" formalism [23-24]. In case of Mg and Be, the only radioactive isotopes suitable for EC-SLI studies are ^{27}Mg (9.45 min) and ^{11}Be (13.8 s). The GaN layers used were specially grown by metal-organic chemical vapour deposition (MOCVD) at the University of Cambridge and based on 4.8 µm thick wurtzite single-crystal GaN epilayers on (0001) sapphire. The first type of sample simply consisted of the not intentionally doped epilayer ("nid-GaN"), while for "*n*-GaN:Si" samples a 150 nm thick layer doped with 1×10^{19} cm^{-3} Si was deposited in addition. Mg predoped samples contained a 150 nm thick top layer doped during growth with 2×10^{19} cm^{-3} Mg. However, while "GaN:Mg" samples were used as-grown, "*p*-GaN:Mg" samples were annealed for 20 min at 800°C under nitrogen atmosphere in order to drive out H and electrically activate the Mg [27].

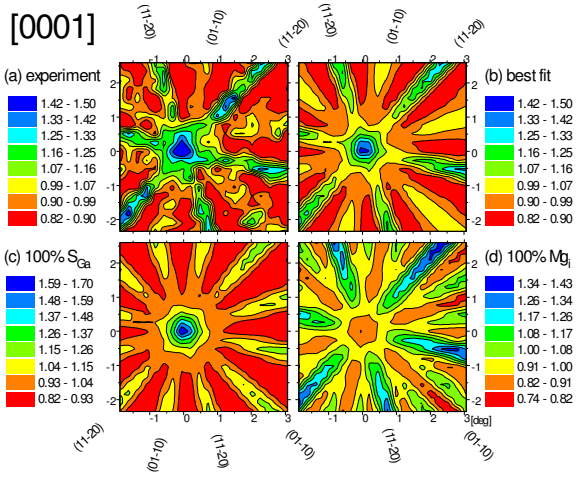

Fig. 1. (a) Experimental ^{27}Mg β^- emission pattern around the [0001] axis of *p*-GaN:Mg during 200°C implantation at a beam current of 0.20 pA, in comparison to (b) the best fit of simulated patterns for 72% aligned with the *c*-axis, e.g. on S_{Ga}, and 31% on the Mg_i interstitial sites near the octahedral position. The theoretical patterns for S_{Ga} and Mg_i sites are shown in panels (c) and (d). From [22].

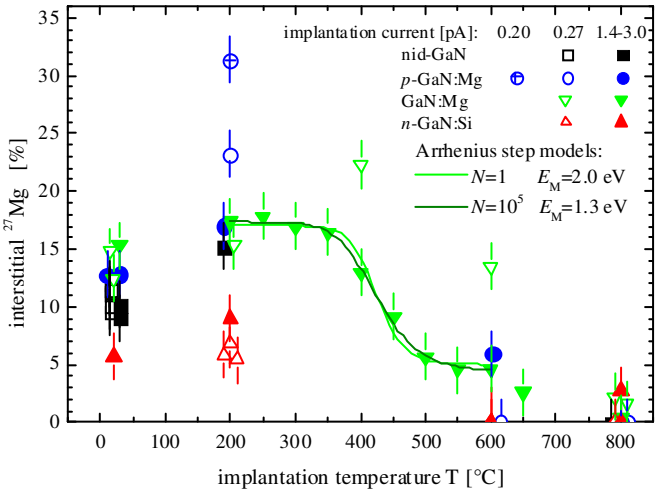

Fig. 2. Interstitial fractions of ^{27}Mg in the four different types of GaN samples as a function of the implantation temperature. Open symbols were implantations at low beam currents of 0.20-0.27 pA, while filled symbols were measured at 1.4-3.0 pA. The solid lines show the fractions using two Arrhenius models: N is the assumed number of jumps required before encountering a Ga vacancy and E_M is the activation energy for migration of interstitial Mg. From [22].

Fig. 1(a) shows the β^- emission distribution around the [0001] axis from ^{27}Mg implanted at 200°C into *p*-GaN:Mg at the very low beam current of 0.20 pA into a 1 mm beam spot, total fluence 1.1×10^{11} cm^{-2}. The fact that the [0001] direction and all major planes exhibit channeling effects proofs that the majority of ^{27}Mg probes are aligned with the *c*-axis. However, comparing the experimental results to the theoretical pattern expected for 100% of ^{27}Mg aligned with the *c*-axis [Fig. 1(c)], one recognizes that the set of [01−10] planes has a lower intensity in comparison to [11−20] planes. This is a consequence of a minority of probes occupying positions in the wide open interstitial region of the wurtzite lattice, such as O, HA, HB or HAB sites since for those sites the (01−10) planes show blocking effects while the (11−20) planes keep the same anisotropy as for sites aligned with the *c*-axis [Fig. 1(d)]. Indeed, the best fit to this experimental pattern was obtained for 31% of Mg on interstitial sites and 72% aligned with the *c*-axis [Fig. 2(b)].

In Fig. 2 the fraction of ^{27}Mg on interstitial Mg_i sites is plotted as a function of the implantation temperature for the four different doping types of GaN, investigated at low and high implantation beam currents. For collecting these data each sample was once oriented with the [0001] facing the detector and then not moved again, only varying the implantation temperature and current, thus assuring maximum reproducibility of emission patterns and good control of the implantation fluence. Samples were first measured using beam currents of 0.20-0.27 pA at 20°C or 200°C, followed by implantations and measurements at higher temperatures, then the beam current was increased to 1.4-3.0 pA and the procedure repeated. Several characteristics are obvious. For measurements within the same beam current series the interstitial ^{27}Mg fraction is clearly correlated with the doping type: interstitial $^{27}Mg_i$ is more prominent in *p*-GaN:Mg than in nid-GaN and lowest in *n*-GaN:Si. The second very clear characteristic is that for high implantation temperatures the interstitial fraction of ^{27}Mg is reduced, reaching in all cases values around 0% at 800°C. Third, for implantations at 200°C into *p*-GaN:Mg, there is a clear and pronounced influence of the fluence visible: during the very first measurement (0.20 pA, Fig. 2) Mg_i reached 31%, dropping to 23% in a subsequent measurement at 0.27 pA; having finished the annealing sequence to 800°C (a temperature at which no more interstitial Mg was found), re-implanting at 200°C with 1.4 pA resulted in 17% Mg_i only. Remarkably, in the case of *n*-GaN:Si, this trend is reversed: for the second sequence of measurements at higher implantation current the initially small fraction of Mgi increased somewhat. Overall, we attribute these fluence-related effects as caused by the introduction of implantation damage, which, as it accumulates, shifts the Fermi level of a sample towards mid gap and also introduces more and more Ga vacancies. While the latter favours the formation of Mg_{Ga} in all samples, the Fermi level shift is of minor consequences in nid-GaN but has opposite effects in *p*- and *n*-type samples (decrease of Mg_i in *p*- but increase in *n*-GaN), which are overlaid on the influence of temperature and doping.

The temperature dependence of the interstitial fraction $f_i(T)$ for high-current implantation into the GaN:Mg sample was used to estimate the migration energy (E_M) of interstitial Mg_i applying two simple Arrhenius models. The models assume that Mg_i that remained interstitial following implantation starts to migrate due to its thermal energy and that it requires a certain number of jumps N until it encounters a Ga vacancy during the life time τ=13.6 min of ^{27}Mg, which will lead to the formation of Mg_{Ga} (see Ref. [20-21] for details):

$$f_i(T) = f_{i0}\exp\left[-\frac{\nu_0\tau}{N}\exp\left(-\frac{E_M}{k_B T}\right)\right].$$

Besides an attempt frequency ν_0, for which we have taken 2×10^{13} Hz, N was assumed either 1 or 10^5, where N=1 represents the limiting case in which the Mg_i has a neighbouring Ga vacancy, and N=10^5 is the upper limit when the diffusion-induced widening of the Mg_i profile becomes comparable to the implantation depth, which can be excluded since it would considerably deteriorate the channeling effects. According to the least square fits for E_M shown by the solid lines in Fig. 2, the migration energies are thus estimated between 2.0 eV (N=1) and 1.3 eV (N=10^5), respectively.

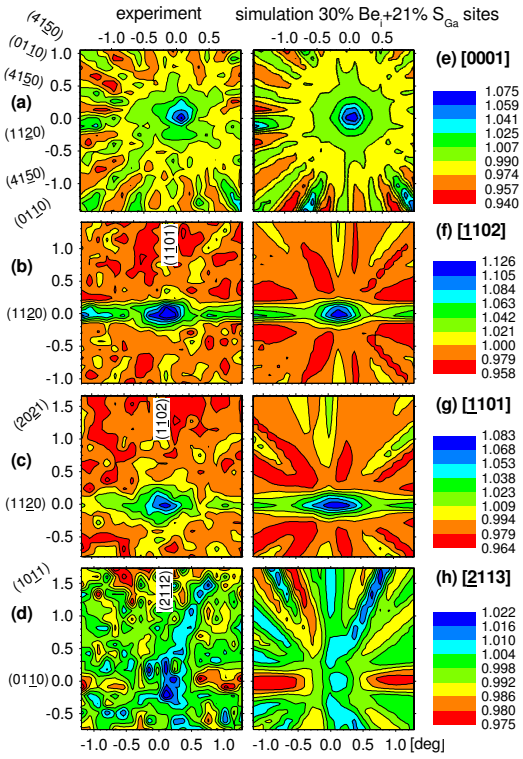

Fig. 3. (a-d) Experimental ^{11}Be β^- emission patterns from nid-GaN during RT implantation, in comparison to (e-h) the best fit of simulated patterns for 21% on S_{Ga}, and 30% on the Be_i interstitial sites near the octahedral position. Fractions are not yet corrected for background, typically this will increase them by a factor of ~2.

Our first test measurements with ^{11}Be implanted at RT in nid-GaN, performed during a parasitic run in 2012, gave encouraging results (Fig. 3). ^{11}Be is a challenging isotope for the EC-SLI method, since due to its high β^- endpoint energy of 11.5 MeV, extensive manybeam simulations at many different energies are required. These simulations have been performed in the meantime and it will be possible to directly analyse future experiments based on them. According to the best fit results in Fig. 3 the majority of Be was actually found on interstitial sites.

Proposed future experiments and summary of requested shifts:

The implementation of the EC-SLI method with ^{27}Mg and ^{11}Be at ISOLDE has for the first time provided an experimental method for direct study of the structural properties of Mg and Be in nitride semiconductors. While this has already lead to valuable results [20-22], the fact that interstitial and substitutional fractions of these implanted probes can now be detected with the precision of a few %, opens further possibilities to investigate how electrical activation processes and radiation damage influence these quantities in differently doped GaN samples. Within a wider picture, our studies also aim at comparing the properties of Mg and Be in nitrides with those of the chemically similar probes ^{8}Li [28], ^{24}Na [21,29-30], ^{42}K, ^{45}Ca [30-31], and ^{89}Sr [30-31], for which emission channeling results are already available. This will allow a systematic correlation of occupied lattice sites and interstitial migration energies with e.g. ionic radii, electronegativity, and other chemical properties.

In the case of ^{27}Mg we would like to concentrate on detailed mapping of the site change from interstitial to substitutional Ga sites in differently doped GaN as a function of implantation temperature and fluence. Particular focus shut be put on further characterizing as-grown GaN:Mg which has not yet been electrically activated by annealing. Here, our first results at low fluence showed a considerable increase in the interstitial Mg fraction upon implantation at 400°C. If this can be confirmed and systematically measured in further experiments, it would allow to study in more detail the processes that take place when Mg-doped GaN:Mg is thermally activated and thus converted to *p*-GaN:Mg. This is commonly associated with the release of H from the sample, hence we will also explore first measurements with intentionally hydrogenated GaN samples. Moreover, precise Arrhenius curves, as are shown for high-fluence implantation in GaN:Mg in Fig. 2, should be measured for other doping types and especially at low implantation currents. This should establish whether the precise site change temperature depends on the doping type of the sample, which would indicate varying activation energies for Mg migration, or differing concentrations of Ga vacancies depending on doping type.

Our shift request assumes two beam times for ^{27}Mg and one for ^{11}Be during the 2-year period 2017+2018 before the ISOLDE shutdown. The total amount of data contained in Fig. 2 was measured during a 4 shift beam time, so a total of 2×8 shifts should be sufficient to perform the

detailed studies outlined above. We would like to point out that dedicated Mg RILIS beam times with a Ti target (the only target that is suitable for our purpose since it allows reducing stable ^{27}Al and radioactive ^{27}Na contaminations to acceptable levels) with less than 2 days duration are usually too short to be accommodated in the ISOLDE schedule.

In 2014, within the last addendum of IS453, INTC had approved 3 shifts for ^{11}Be experiments. However, such a minor amount of shifts could not be scheduled in the years 2014-2016. Therefore, the only data we have measured so far are shown in Fig. 3 and concern RT implantation into GaN. These were achieved during a parasitic run in 2012 during the times when the primary user did not take beam. For ^{11}Be we aim at establishing at which temperature the site changes to substitutional sites occur in undoped nid-GaN, *p*-GaN:Mg and in AlN, which should take ~8 shifts, since ^{11}Be yields are lower than ^{27}Mg. This will allow assessing the relevance of interstitial Be_i as compensating centers, and first experimental values for the interstitial migration energy of Be_i in these materials, for which theoretical predictions in GaN suggest $E_M(Be_i)$=1.2-2.9 eV [15].

Table1: Number of shifts requested for each isotope

isotope	yield (atoms/μC)	target – ion source	Shifts (8h)
^{27}Mg	1×10^7	Ti-W – RILIS Mg	16
^{11}Be	6×10^6	UC_x-W or Ta-W – RILIS Be	8
		Total shifts:	**24**

References:

[1] I. Akasaki, "Nobel Lecture: Fascinated journeys into blue light", Rev. Mod. Phys. 87 (2015) 1119.

[2] H. Amano, "Nobel Lecture: Growth of GaN on sapphire via low-temperature deposited buffer layer and realization of *p*-type GaN by Mg doping followed by low-energy electron beam irradiation", Rev. Mod. Phys. 87 (2015) 1133.

[3] S. Nakamura, "Nobel Lecture: Background story of the invention of efficient blue InGaN light emitting diodes", Rev. Mod. Phys. 87 (2015) 1139.

[4] S. Brochen, J. Brault, S. Chenot, A. Dussaigne, M. Leroux, B. Damilano, "Dependence of the Mg-related acceptor ionization energy with the acceptor concentration in *p*-type GaN layers grown by molecular beam epitaxy", Appl. Phys. Lett. 103 (2013) 032102.

[5] J. Neugebauer, C.G. Van de Walle, "Theory of point defects and complexes in GaN", Proc. Mater. Res. Soc. Symp. 395 (1996) 645.

[6] C.G. Van de Walle J. Neugebauer, "First-principles calculations for defects and impurities: Applications to III-nitrides", J. Appl. Phys. 95 (2004) 3851.

[7] F.A. Reboredo, S.T. Pantelides: "Novel defect complexes and their role in the *p*-type doping of GaN", Phys. Rev. Lett 82 (1999) 1887.

[8] J.L. Lyons, A. Janotti, C.G. Van de Walle, "Shallow versus deep nature of Mg acceptors in nitride semiconductors", Phys. Rev. Lett. 108 (2012) 156403.

[9] Q. Yan, A. Janotti, M. Scheffler, C.G. Van de Walle, "Role of nitrogen vacancies in the luminescence of Mg-doped GaN", Appl. Phys. Lett. 100 (2012) 142110.

[10] J. Buckeridge, C.R.A. Catlow, D.O. Scanlon, T.W. Keal, P. Sherwood, M. Miskufova, A. Walsh, S.M. Woodley, A.A. Sokol, "Determination of the nitrogen vacancy as a shallow compensating center in GaN doped with divalent metals", Phys. Rev. Lett. 114 (2015) 016405.

[11] S. Hautakangas, J. Oila, M. Alatalo, K. Saarinen, L. Liszkay, D. Seghier H.P. Gislason, "Vacancy defects as compensating centers in Mg-doped GaN", Phys. Rev. Lett. 90 (2003) 137402.

[12] C.D. Latham, R. Jones, S. Öberg, R.M. Nieminen, P.R. Briddon, "Calculated properties of nitrogen-vacancy complexes in beryllium- and magnesium-doped GaN", Phys. Rev. B 68 (2003) 205209.

[13] G. Miceli, A. Pasquarello, "Self-compensation due to point defects in Mg-doped GaN", Phys. Rev. B 93 (2016) 165207.

[14] M.A. Reshchikov, D.O. Demchenko, J.D. McNamara, S. Fernández-Garrido, R. Calarco, "Green luminescence in Mg-doped GaN", Phys. Rev. B 90 (2014) 035207.

[15] C.G. Van de Walle, S. Limpijumnong, J. Neugebauer, "First-principles studies of beryllium doping of GaN", Phys. Rev. B 63 (2001) 245205

[16] C.D. Latham, R.M. Nieminen, C.J. Fall, R. Jones, S. Öberg, P.R. Briddon "Calculated properties of point defects in Be-doped GaN", Phys. Rev. B 67 (2003) 205206.

[17] S. Lany, A. Zunger, "Dual nature of acceptors in GaN and ZnO: The curious case of the shallow Mg_{Ga} deep state", Appl. Phys. Lett. 96 (2010) 142114.

[18] J. L. Lyons, A. Janotti, C.G. Van de Walle, "Effects of hole localization on limiting *p*-type conductivity in oxide and nitride semiconductors", J. Appl. Phys. 115 (2014) 012014.

[19] K. Lawniczak-Jablonska, T. Suski, I. Gorczyca, N. Christensen, J. Libera, J. Kachniarz, P. Lagarde, R. Cortes, I. Grzegory, "Anisotropy of atomic bonds formed by *p*-type dopants in bulk GaN crystals", Appl. Phys. A 75 (2002) 577.

[20] L.M. Amorim, U. Wahl, L. Pereira, S. Decoster, D.J. Silva, M.R. da Silva, A. Gottberg, J.G. Correia, K. Temst, A. Vantomme, Appl. Phys. Lett. 103 (2013) 262102; https://cds.cern.ch/record/1641212/files/CERN-OPEN-2014-013.pdf.

[21] L.M. Amorim, "Lattice site location of electrical dopant impurities in group-III nitrides", PhD thesis, KU Leuven, Belgium (2016). CERN-THESIS-2016-226; https://cds.cern.ch/record/2240696.

[22] U. Wahl, L.M. Amorim, V. Augustyns, A. Costa, E. David-Bosne, T.A.L. Lima, G. Lippertz, J.G. Correia, M.R. da Silva, M.J. Kappers, K. Temst, A.Vantomme, L.M.C. Pereira, "Lattice location of Mg in GaN: a fresh look at doping limitations", accepted by Phys. Rev. Lett.

[23] H. Hofsäss, G. Lindner, "Emission channeling and blocking", Physics Reports 201 (1991) 121.

[24] U. Wahl, "Advances in electron emission channeling measurements in semiconductors", Hyperfine Interactions 129 (2000) 349; https://cds.cern.ch/record/638167/files/open-2003-029.pdf.

[25] U. Wahl, J.G. Correia, A. Czermak, S. Jahn, P. Jalocha, J. Marques, A. Rudge, F. Schopper, J.C. Soares, A. Vantomme, "Position-sensitive Si pad detectors for electron emission channeling experiments", Nucl. Instr. Meth. A 524 (2004) 245; https://cds.cern.ch/record/985886/files/open-2006-045.pdf.

[26] M.R. Silva, U. Wahl, J.G. Correia, L.M. Amorim, L.M.C. Pereira, "A versatile apparatus for on-line emission channeling experiments", Rev. Sci. Instrum. 84 (2013) 073506; https://cds.cern.ch/record/1640598/files/CERN-OPEN-2014-005.pdf.

[27] R.A. Oliver, F.C.P. Massabuau, M.J. Kappers, W.A. Phillips, E.J. Thrush, C.C. Tartan, W.E. Blenkhorn, T.J. Badcock, P. Dawson, M.A. Hopkins, D.W.E. Allsopp, C.J. Humphreys, "The impact of gross well width fluctuations on the efficiency of GaN-based light emitting diodes", Appl. Phys. Lett. 103 (2013) 141114.

[28] M. Dalmer, M. Restle, M. Sebastian, U. Vetter, H. Hofsäss, M. D. Bremser, C. Ronning, R. F. Davis, U. Wahl, K. Bharuth-Ram, and the ISOLDE collaboration, "Lattice site location studies of ion implanted ^{8}Li in GaN", J. Appl. Phys. 84, 3085 (1998).

[29] C. Ronning, M. Dalmer, M. Uhrmacher, M. Restle, U. Vetter, L. Ziegeler, H. Hofsäss, T. Gehrke, K. Jarrendahl, R.F. Davis, ISOLDE collaboration, "Ion implanted dopants in GaN and AlN: Lattice sites, annealing behavior, and defect recovery", J. Appl. Phys. 87, 2149 (2000).

[30] B. De Vries, "Lattice site location of impurities in group-III nitrides using emission channeling", PhD thesis, KU Leuven, Belgium (2006); CERN-THESIS-2005-102; http://cds.cern.ch/record/1640588.

[31] B. De Vries, A. Vantomme, U. Wahl, J.G. Correia, J.P. Araújo, W. Lojkowski, D. Kolesnikov, and the ISOLDE collaboration, "Lattice site location and annealing behavior of implanted Ca and Sr in GaN", J. Appl. Phys. 100, 023531 (2006); https://cds.cern.ch/record/985357/files/open-2006-044.pdf.

Appendix

DESCRIPTION OF THE PROPOSED EXPERIMENT

The experimental setup comprises:
EC-SLI on-line implantation and measurement chamber at ISOLDE GPS-GHM beam line

Part of the Choose an item.	Availability	Design and manufacturing
EC-SLI, on-line emission channeling chamber at GHM	☒ Existing	☒ To be used without any modification
[insert lines if needed]		

HAZARDS GENERATED BY THE EXPERIMENT

(if using fixed installation) Hazards named in the document relevant for the fixed installation. [EC-SLI, On-line Emission Channeling Chamber at GHM]

Additional hazards:

Hazards			
	EC-SLI Chamber at GHM		
Thermodynamic and fluidic			
Pressure	[-][Bar], [-][l]		
Vacuum	10^{-6} mbar, 70 l		
Temperature	[Room temperature] [K]		
Heat transfer			
Thermal properties of materials	At the sample holder inside the chamber, under vacuum, there is an annealing system up to 1173 K. A closed cycle refrigerator can cool samples down to 50 K		
Cryogenic fluid	[He gas], [13][Bar], [3][l] Closed cycle He refrigerator		
Electrical and electromagnetic			
Electricity	[220] [V], [25][A]		
Static electricity			
Magnetic field	[magnetic field] [T]		
Batteries	☐		
Capacitors	☐		
Ionizing radiation			
Target material	Solid-state ,single crystal samples for analysis, mounted into a goniometer under vacuum. The short-lived isotopes are directly implanted into the sample and measurements are done in situ.		
Beam particle type (e, p, ions, etc)	Isolde radioactive ion beams		
Beam intensity	From pA to nA		
Beam energy	From 30 to 60 keV		
Cooling liquids	[liquid]		
Gases	[gas]		
Calibration sources:	☒ calibrations are done on-line with real samples during		

	the runs, or using weak sources implanted with long lived isotopes, e, g, 73 As (80d – c.e. emitter) or 59Fe (44.5d – β-emitter)		
• Open source	☒ 27Mg (9.5 min) *1.2MBq (satur.)* 11Be (13.8 s) *0.8MBq (satur.)*		
• Sealed source	☐ [ISO standard]		
• Isotope			
• Activity			
Use of activated material:			
• Description	☐		
• Dose rate on contact and in 10 cm distance	Max. 500 µSv/h at contact at the chamber walls, during experiments, depending on isotope and yield. Typical is ~100 µSv/h on contact. at the chamber walls, ~50 µSv/h in 10 cm distance. The chamber is enclosed by concrete blocks that shield radiation at the working zones to ambient background of the ISOLDE hall, < 5 µSv/h. Experiments are remotely monitored.		
• Isotope			
• Activity			
Non-ionizing radiation			
Laser			
UV light			
Microwaves (300MHz-30 GHz)			
Radiofrequency (1-300MHz)			
Chemical			
Toxic	[chemical agent], [quantity]		
Harmful	[chemical agent], [quantity]		
CMR (carcinogens, mutagens and substances toxic to reproduction)	[chemical agent], [quantity]		
Corrosive	[chemical agent], [quantity]		
Irritant	[chemical agent], [quantity]		
Flammable	[chemical agent], [quantity]		
Oxidizing	[chemical agent], [quantity]		
Explosiveness	[chemical agent], [quantity]		
Asphyxiant	[chemical agent], [quantity]		
Dangerous for the environment	[chemical agent], [quantity]		
Mechanical			
Physical impact or mechanical energy (moving parts)	[location]		
Mechanical properties (Sharp, rough, slippery)	[location]		
Vibration	[location]		
Vehicles and Means of Transport	[location]		
Noise			

Frequency	[frequency],[Hz]		
Intensity			
Physical			
Confined spaces	[location]		
High workplaces	[location]		
Access to high workplaces	[location]		
Obstructions in passageways	[location]		
Manual handling	[location]		
Poor ergonomics	[location]		

0.1 Hazard identification

3.2 Average electrical power requirements (excluding fixed ISOLDE-installation mentioned above): *(make a rough estimate of the total power consumption of the additional equipment used in the experiment)*

About 5 kW for the on-line chamber at GHM. Each of the 3 off-line setups about 2 kW.